CrossMark

ICPPP 18

Laser-Generated Rayleigh Waves Propagating in Transparent Viscoelastic Adhesive Coating/Metal Substrate Systems

Yi-jun Guan[1] · Hong-xiang Sun[1,2,3] ·
Shou-qi Yuan[1] · Shu-yi Zhang[2] · Yong Ge[1]

Abstract We have established numerical models for simulating laser-generated Rayleigh waves in coating/substrate systems by a finite element method and investigated the propagation characteristics of Rayleigh waves in systems concerning the viscoelasticity and transparency of adhesive coatings. In this way, we have studied the influence of the mechanical properties of the coating, such as the elastic moduli, viscoelastic moduli, coating thickness, transparency, and coating material, on the propagation characteristics of the Rayleigh waves. The results show that the propagation characteristics of the Rayleigh waves can be divided into low- and high-frequency parts. The high-frequency propagation characteristics of the Rayleigh wave are closely related to the properties of the adhesive coating.

Keywords Coating/substrate structure · Finite element method · Laser ultrasound · Rayleigh wave · Viscoelasticity

✉ Hong-xiang Sun
  jsdxshx@ujs.edu.cn

1   Faculty of Science, Research Center of Fluid Machinery Engineering and Technology, Jiangsu University, Zhenjiang 212013, China

2   Laboratory of Modern Acoustics, Institute of Acoustics, Collaborative Innovation Center of Advanced Microstructures, Nanjing University, Nanjing 210093, China

3   State Key Laboratory of Acoustics, Institute of Acoustics, Chinese Academy of Sciences, Beijing 100190, China

1 Introduction

Adhesive coating/substrate structures are widely used in the fields of aerospace industry, micro–nanodevices, and civil engineering structural strengthening and repairing, etc. The adhesive quality of a system is mainly determined by the mechanical properties of the adhesive layer [1,2]. In past studies, adhesive coatings were considered as elastic materials. This is because the mechanical properties of solid adhesive coatings are close to those of the elastic solids, and because on that way, theoretical calculations can be simplified. In practice, shockproof adhesive coatings, nonsolid adhesive coatings, and hyperthermal adhesive coatings cannot be regarded as elastic solids due to attenuation effects induced by their viscoelasticity.

The laser ultrasound technique has potential applications in nondestructive evaluations and characterizations of various structures [3–9]. In adhesive coating/substrate structures, the features of laser-generated ultrasonic waves depend not only on the properties of the adhesive layer, but also on those of the substrate, so that the characteristics of the laser-generated ultrasonic waves become more difficult to interpret. In this field, Rokhlin et al. [10] studied the equivalent boundary conditions for a thin epoxy resin layer between solids. They showed that a very thin lower density layer can be evaluated by a spring model. Heller et al. [11] used a two-dimensional Fourier transform to evaluate the stiffness of an adhesive layer, and they measured Lamb waves in layered plates to study the influence of the adhesive layer on the dispersions. Cheng et al. [1] simulated laser-generated Rayleigh waves in an elastic adhesive coating/substrate in Hankel and Laplace transform domain by using a Thompson transfer matrix approach, and they obtained waveforms in the time domain through a numerical inverse transform. Liu et al. [2] adopted a laser-induced grating technique to generate narrow band surface waves in an epoxy-bonded copper–aluminum layered structure. They introduced an inverse algorithm based on the simplex method to determine the thickness and elastic properties of the adhesive layer. The aforementioned works showed that the laser ultrasound technique is a powerful tool in the evaluation of the adhesive quality. However, till now the adhesive layer has been considered as a purely elastic and opaque material.

Constitutive relations developed in frequency domain and complex moduli representing the viscoelastic property can properly describe the dynamic behavior of composite materials [12]. Several cases of laser-generated ultrasonic waves in single-layer plates [13–15], coating/substrate systems [16,17], and sandwich structures [18,19] made of viscoelastic materials have been modeled successfully. However, little work has been published so far on the laser-generated Rayleigh waves in the transparent viscoelastic adhesive coating/substrate systems.

In this work, finite element (FE) models are developed to numerically study laser-generated Rayleigh waves in epoxy coating/aluminum substrate systems. We study the influence of the mechanical properties of the coating, such as the elastic moduli, viscoelastic moduli, coating thickness, transparency, and material, on the propagation characteristics of the Rayleigh waves in detail. This study provides a theoretical basis for extracting mechanical parameters and evaluating the adhesive quality of the viscoelastic adhesive coating/substrate structures.

2 Plane Strain Theory

The geometry of pulsed linear laser irradiation on a transparent viscoelastic adhesive coating/metal substrate system is schematically shown in Fig. 1a. Epoxy (Ep) and aluminum (Al) are used as the coating and substrate, respectively. The coordinates x, y, and z are chosen to be parallel to the principal axes of the structure. The propagation direction of the Rayleigh wave is along the x-axis. The optical axis of the focused laser pulse irradiation is along the y-axis. The pulse laser line source is along the z-axis, producing displacements in the x and y direction. The geometry can be simplified as a two-dimensional model shown in Fig. 1b, in which the symmetrical left half is omitted. Due to the transparency of the Ep coating, the laser source is located at the position $x = 0$ on the surface of the Al substrate. The absorbing regions (AR) are located at the right and bottom sides [16]. The governing equations of motion in the coating and substrate can be expressed in the frequency domain as follows [13]

$$\begin{cases} C_{11}^* \frac{\partial^2 \tilde{u}}{\partial x^2} + C_{66}^* \frac{\partial^2 \tilde{u}}{\partial y^2} + (C_{12}^* + C_{66}^*) \frac{\partial^2 \tilde{v}}{\partial x \partial y} + \rho \omega^2 \tilde{u} = 0 \\ C_{22}^* \frac{\partial^2 \tilde{v}}{\partial y^2} + C_{66}^* \frac{\partial^2 \tilde{v}}{\partial x^2} + (C_{12}^* + C_{66}^*) \frac{\partial^2 \tilde{u}}{\partial x \partial y} + \rho \omega^2 \tilde{v} = 0 \end{cases}, \tag{1}$$

where ρ is the density, ω is the angular frequency, and $\tilde{u}$ and $\tilde{v}$ are the Fourier transforms of the displacements in the x and y directions, respectively. $C_{ij}^* = C_{ij}' + iC_{ij}''$ (i, $j = 1, 2, \ldots, 6$) are the viscoelastic moduli, in which C_{ij}' and C_{ij}'' are the elastic and viscous moduli, respectively. In the Ep/Al system, $C_{ij}^* = C_{ij}' + iC_{ij}''$ are adopted for the viscoelastic Ep coating, but C_{ij}^* are simplified as C_{ij}' for the elastic Al substrate.

3 FE Model and Parameters

A FE model was constructed to numerically simulate the laser-generated Rayleigh wave in the Ep/Al system by COMSOL Multiphysics software. Equation 1 can be written in the following FE-code form [20]

$$\nabla \cdot (c \nabla \tilde{U}) - a\tilde{U} = 0, \tag{2}$$

where $\nabla = \left(\frac{\partial}{\partial x}, \frac{\partial}{\partial y} \right)$, $\tilde{U} = (\tilde{u}, \tilde{v})$, c is a 2×2 matrix composed of four sub-matrices expressed as

$$\begin{aligned} c_{11} = \begin{pmatrix} C_{11}^* & 0 \\ 0 & C_{66}^* \end{pmatrix} & \quad c_{12} = \begin{pmatrix} 0 & C_{12}^* \\ C_{66}^* & 0 \end{pmatrix} \\ c_{21} = \begin{pmatrix} 0 & C_{66}^* \\ C_{12}^* & 0 \end{pmatrix} & \quad c_{22} = \begin{pmatrix} C_{66}^* & 0 \\ 0 & C_{22}^* \end{pmatrix} \end{aligned}, \tag{3}$$

and a is a 2×2 matrix given by

$$a = \begin{pmatrix} -\rho\omega^2 & 0 \\ 0 & -\rho\omega^2 \end{pmatrix}. \tag{4}$$
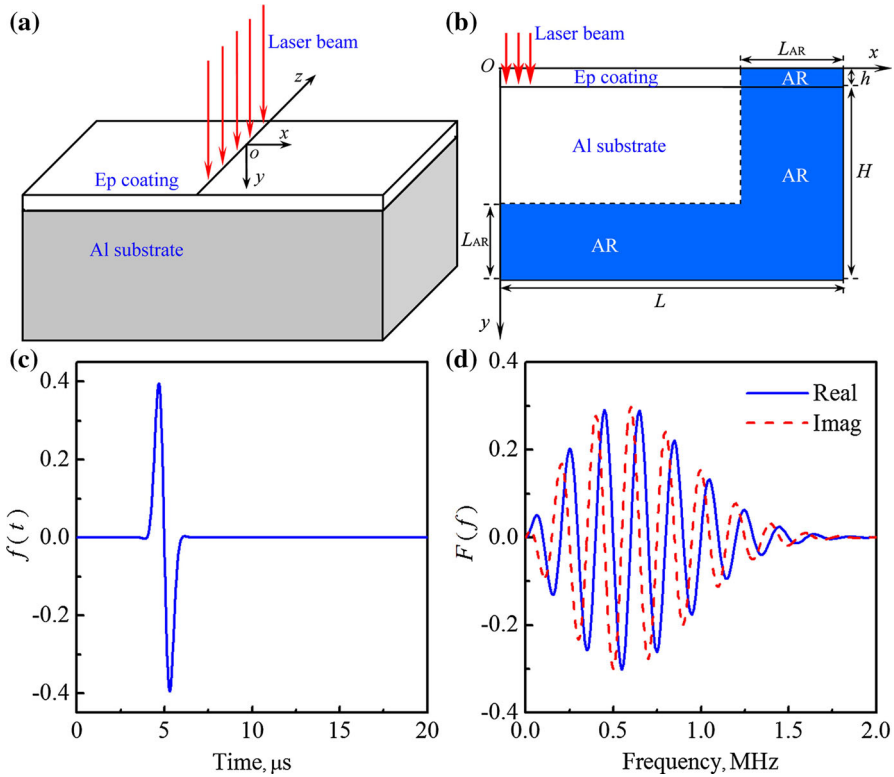
Fig. 1 (a) Geometry diagram of numerical model and (b) cross section of sample. (c) Time history of the exciting source and (d) its frequency spectrum

The stress tensors and displacements are taken to be continuous at all informal interfaces, and stress-free boundary conditions are assumed at the surfaces. The initial displacement, velocity, and acceleration are zero.

In the simulations, the geometrical parameters shown in Fig. 1b were chosen as follows: $h = 0.2$ mm, $H = 30$ mm, $L = 40$ mm, and $L_{AR} = 10$ mm. The material parameters were taken as $\rho = 1100$ kg·m^{-3}, $C_{11}^* = C_{22}^* = 7.0 + i*0.21$ GPa, $C_{12}^* = 4.8 + i*0.14$ GPa, and $C_{66}^* = 1.1 + i*0.03$ GPa for the Ep [18] and $\rho = 2780$ kg·m^{-3}, $C_{11}^* = C_{22}^* = 112$ GPa, $C_{12}^* = 58$ GPa, and $C_{66}^* = 27$ GPa for the Al.

The equivalent stress induced by the laser pulse was adopted as an exciting source, which is described as [16,21]

$$f(t) = \frac{2}{\alpha\sqrt{2\pi}} \exp\left[-\frac{(t-t_0)^2}{2\alpha^2}\omega_c^2\right] \sin(\omega_c t), \qquad (5)$$

where α is a dimensionless parameter controlling the pulse width, t_0 determines the pulse delay time, and $\omega_c = 2\pi f_c$ is the center angular frequency of the pulse. Figure 1c, d shows the waveforms of the pulse source and its frequency spectrum, $f(t)$ and $F(f)$, respectively, and the parameters were $\alpha = 1.2$, $t_0 = 5\,\mu$s, and $f_c = 0.5$ MHz.
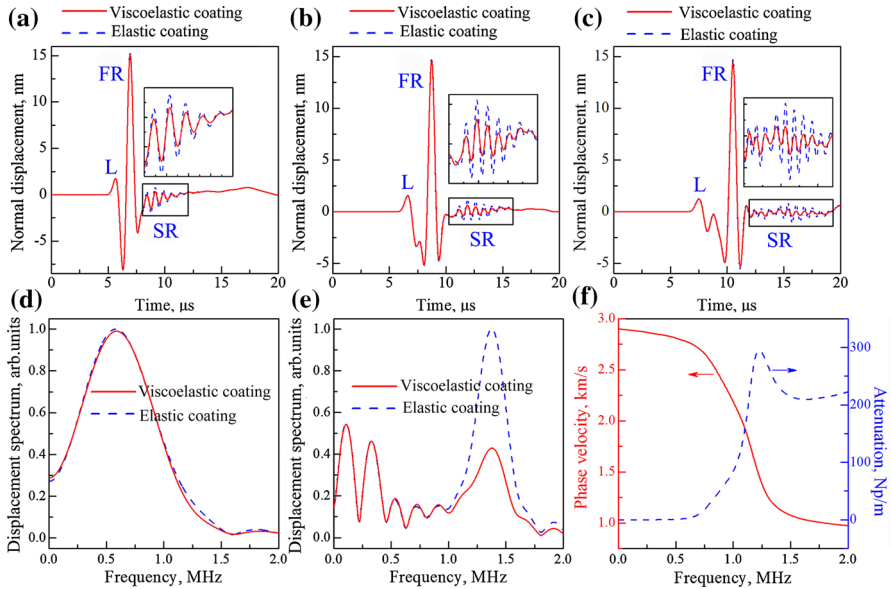
Fig. 2 Normal surface displacements in Ep/Al system with source–receiver distances of (a) 5 mm, (b) 10 mm, and (c) 15 mm; displacement spectra of (d) FR and (e) SR with source–receiver distance of 10 mm; and (f) phase velocity and attenuation curves of Rayleigh wave in Ep/Al system

In the FE model, the element size was generally arranged to be 20 μm, and 5 μm near the exciting zone. The spectrum $F(f)$ of the exciting source was confined to $0 \leq f \leq 2.0$ MHz as shown in Fig. 1d. In the simulations, the frequency scanning step was arranged to be 0.01 MHz, so the frequency range of $F(f)$ was divided into 200 components. Temporal displacement waveforms were obtained by applying an inverse fast Fourier transform (iFFT) of the displacement spectra.

4 Numerical Results and Discussion

4.1 Propagation Characteristics of Rayleigh Waves in Ep/Al System

As a first example, we have determined the normal surface displacement with the source–receiver distances of 5 mm, 10 mm, and 15 mm in the Ep/Al system. The solid and dashed lines in Fig. 2a–c represent the waveforms for the Ep coating with and without viscoelasticity, respectively. The longitudinal wave (L) and the Rayleigh wave (R) are dominant. The first arriving part of the Rayleigh wave (FR) mainly propagates in the Al substrate with high velocity and is not affected by the properties of the coating. The later arriving wave (SR) propagates in Ep coating with low velocity and is dispersive. The amplitude of SR decreases gradually with the increase in the source–receiver distance (solid lines), as a result of the viscoelasticity of the Ep.

Figure 2d, e shows the displacement spectra of the FR and SR in Fig. 2b, respectively. The energy of the FR is mainly below 1.0 MHz with the center 0.55 MHz,

while the energy of the SR is mainly in the range 1.0 MHz–1.7 MHz with the center 1.4 MHz. Compared with the results for the Ep coating without viscoelasticity (dashed lines), the spectra of the FR (Fig. 2d) almost remain unchanged, but the amplitudes of the SR (Fig. 2e) are much smaller in the frequency range 1.0 MHz–1.7 MHz for the Ep coating with viscoelasticity (solid lines). The attenuation of the SR is different at various frequencies, and the maximum attenuation appears at 1.35 MHz.

To explain the mechanism of this phenomenon, we have calculated the phase velocity and attenuation curves of the Rayleigh wave in the Ep/Al system with the viscoelasticity of the Ep, which is shown in Fig. 2f. Below 0.75 MHz, the phase velocity is almost constant and the attenuation coefficient induced by the viscoelasticity tends to zero. Therefore, the waveform and spectrum of the FR keep constant and nondispersive characteristics, further indicating that the FR propagates mainly in the substrate. On the other hand, in the range 1.0 MHz–1.7 MHz, the phase velocity decreases and the attenuation coefficient increases to reach a maximum at 1.4 MHz, which indicates that the propagation characteristics of the SR are determined strongly by the properties of the viscoelastic Ep coating.

4.2 Effects of Mechanical Parameters of Ep Coating on SR Propagation Characteristics

In this section, we discuss the effects of the viscoelastic moduli, elastic moduli, thickness, and transparency of the Ep coating on the propagation characteristics of the SR in the Ep/Al system, for a source–receiver distance of 10 mm.

We simulated the normal surface displacements for varying the viscous moduli C_{ij}'' of the Ep coating m times (from 0 to 1.5), while keeping the elastic moduli C_{ij}' unchanged, as shown in Fig. 3a, b. The spectra of the SR in Fig. 3a and b are shown in Fig. 3c and d, respectively. With increasing m, the dispersive characteristic of the SR is almost unchanged, but the amplitude decreases gradually. Figure 3e, f shows the phase velocity and attenuation curves of the Rayleigh wave, in which the values of m are 0.5, 1.0, and 1.5. The phase velocity curves are not affected by the increase in the coating damping. However, with increasing m, the attenuation becomes stronger in the range 1.0 MHz–2.0 MHz, and a maximum appears at about 1.25 MHz, but the attenuation closes to zero below 0.75 MHz. The viscoelasticity has no effect on the velocity and dispersive characteristic, but has a great influence on the attenuation characteristic of the Rayleigh wave, which agrees well with the results in Fig. 3a, b.

Figure 4a, b shows the normal surface displacements for C_{ij}' varying as C_{ij}'' of the Ep coating, while keeping C_{ij}'' unchanged. Figure 4a, b shows that, with the increase of n (from 0.75 to 1.25), the velocity of the SR increases apparently, but the dispersive characteristic and attenuation of SR become weaker. The characteristics of the SR are thus also determined by the elastic moduli of the Ep coating. Figure 4c, d presents the spectra of the SR, which is corresponding to Fig. 4a and b, respectively. With the increase of n, the range of SR moves to higher frequency region, and the attenuation of the SR becomes weaker.

Figure 4e, f presents the phase velocity and attenuation curves of the Rayleigh wave, and the values of n are 0.5, 1.0, and 1.5, respectively. With the increase of n,
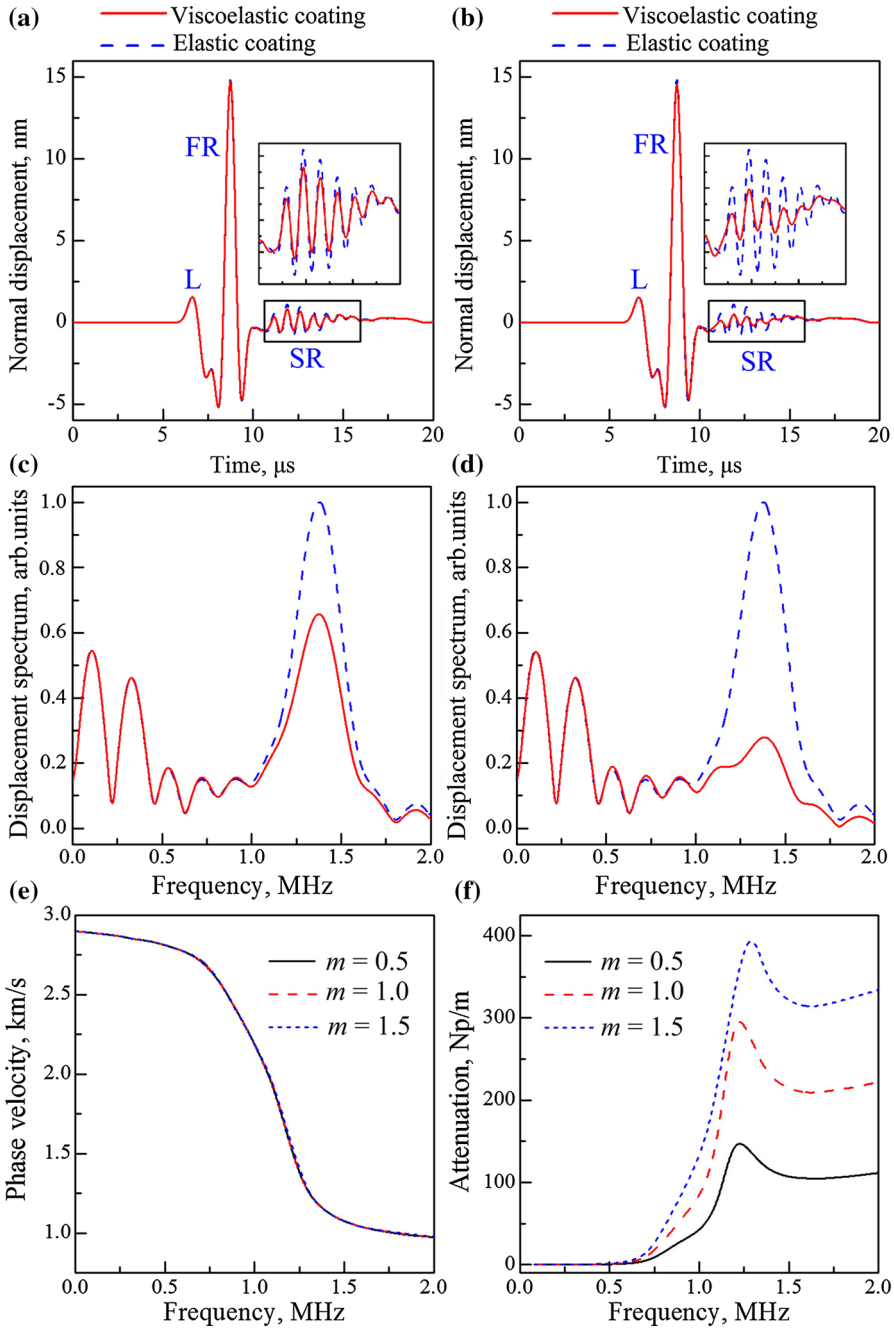
Fig. 3 Normal surface displacements with m times of C_{ij}'' of Ep coating: (a) $m = 0.5$ and (b) $m = 1.5$; displacement spectra of SR: (c) $m = 0.5$ and (d) $m = 1.5$; and (e) phase velocity and (f) attenuation curves of Rayleigh wave in Ep/Al system with m times of C_{ij}'' of Ep coating
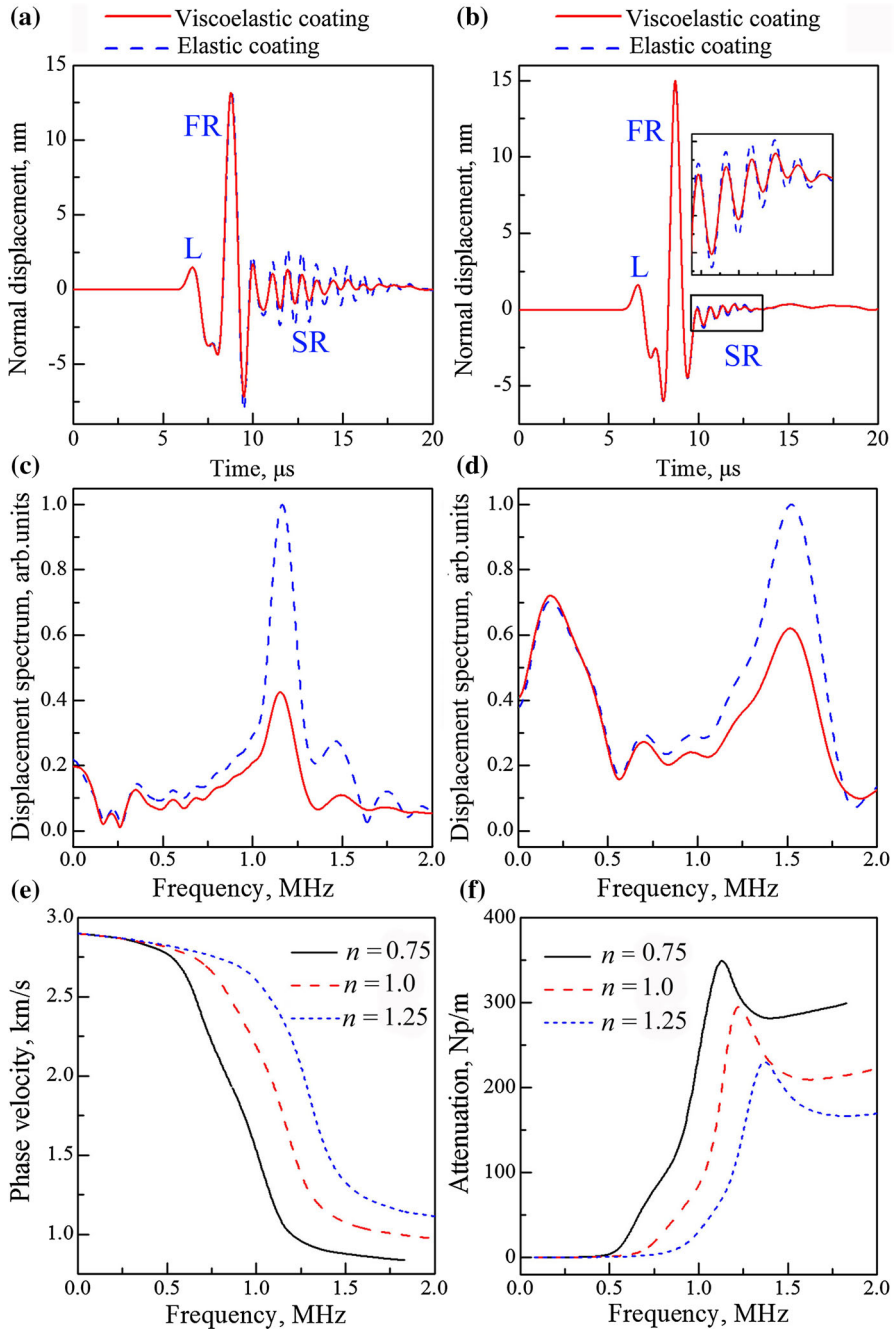
Fig. 4 Normal surface displacements with n times of C'_{ij} of Ep coating: (a) $n = 0.75$ and (b) $n = 1.25$; displacement spectra of SR: (c) $n = 0.75$ and (d) $n = 1.25$; and (e) phase velocity and (f) attenuation curves of Rayleigh wave in Ep/Al system with n times of C'_{ij} of Ep coating
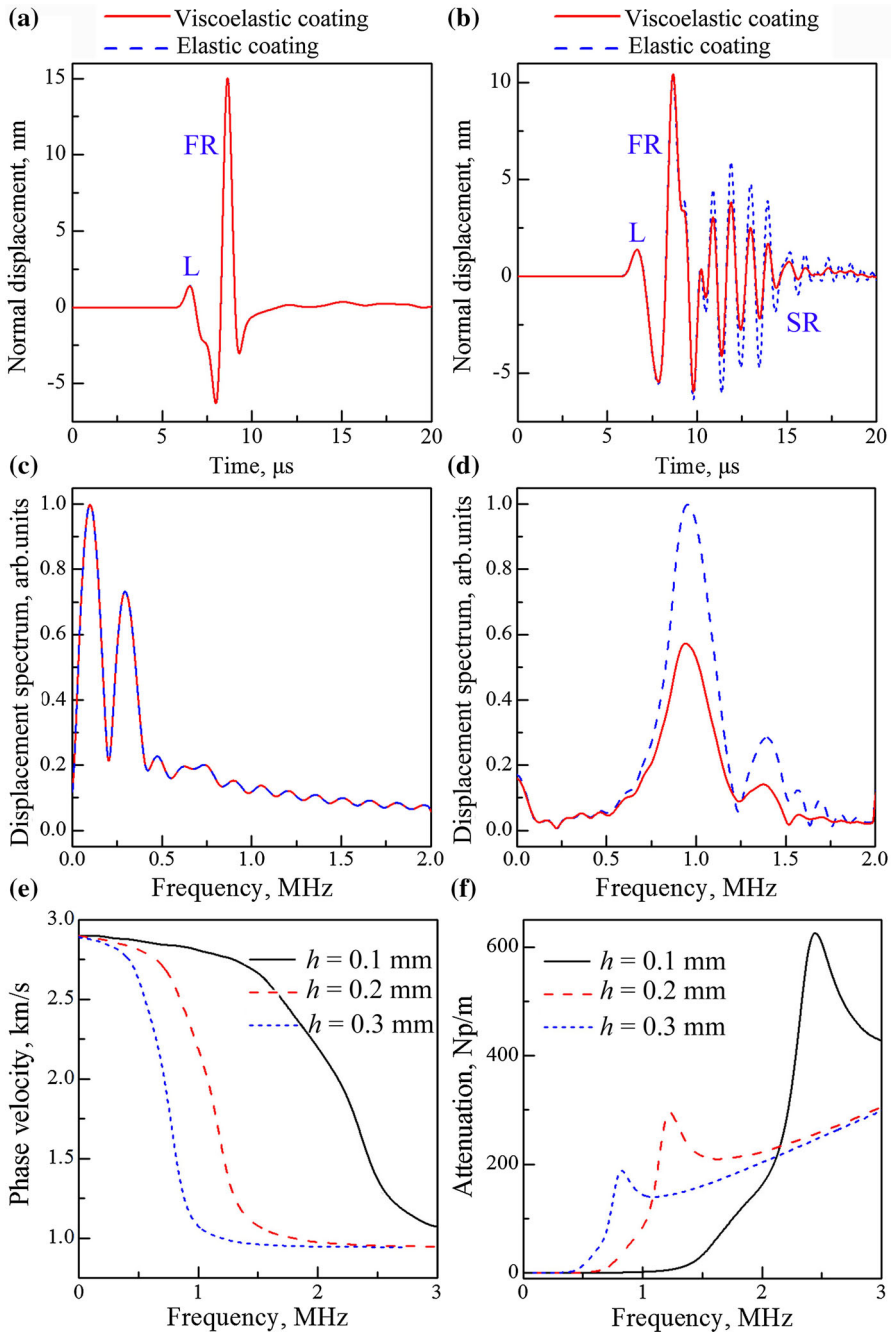
Fig. 5 Normal surface displacements with different coating thicknesses: (a) $h = 0.10$ mm and (b) $h = 0.30$ mm; displacement spectra of SR: (c) $h = 0.10$ mm and (d) $h = 0.30$ mm; and (e) phase velocity and (f) attenuation curves of Rayleigh wave in Ep/Al system with different coating thicknesses
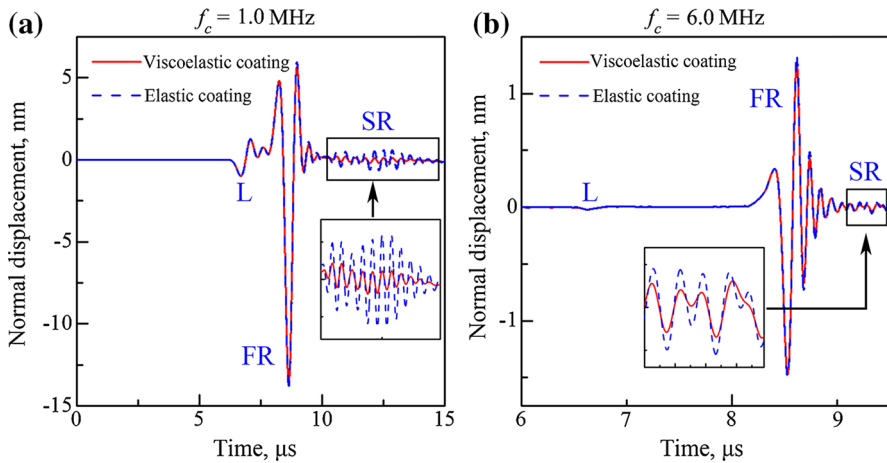
Fig. 6 Normal surface displacements with different coating thicknesses (a) $h = 0.10$ mm and (b) $h = 0.02$ mm

the phase velocity of the Rayleigh wave increases as the frequency exceeds 0.5 MHz. The attenuation of the SR decreases, and the peak of the attenuation curve moves to the higher frequency region, which agrees well with the results obtained in Fig. 4c, d. The above results indicate that the propagation characteristics (velocity, dispersion, and attenuation) of the SR are related to the elastic moduli of the coating.

Also, the influence of the coating thickness (h) on the propagation characteristics of the SR was investigated. Figure 5a, b shows the normal surface displacements of the Rayleigh wave with different values of h. The spectra of the transient waveforms in the time range of $10\,\mu s-20\,\mu s$ in Fig. 5a and b are presented in Fig. 5c and d, respectively. The SR does not exist in the simulation frequency range, since h is too small. However, with increasing h, the dispersive characteristic of the SR appears as shown in Figs. 2b and 5b. Moreover, it can be obtained from Figs. 2e and 5d that the center frequency of the SR decreases with the increase of h. The effect of h on the phase velocity is shown in Fig. 5e, in which h are 0.1 mm, 0.2 mm, and 0.3 mm, respectively. With increasing h, the phase velocity decreases, and the waveform of the SR shows more apparent dispersive characteristics. The attenuation curves for the three cases are given in Fig. 5f. With increasing h, the attenuation decreases gradually, and the peak of the attenuation curves moves to the lower frequency region. The characteristics of the SR are thus closely related to h.

To show the characteristics of Rayleigh waves in Ep/Al system with smaller coating thickness, we have simulated the normal surface displacements in the following two cases: (1) $h = 0.10$ mm and $f_c = 1.0$ MHz and (2) $h = 0.02$ mm and $f_c = 6.0$ MHz. As shown in Fig. 6a, with higher center frequency f_c, the SR appears, and its attenuation and dispersive characteristics are similar as those in Fig. 2b. Besides, as shown in Fig. 6b, the SR in the Ep/Al system with coating thickness 0.02 mm is excited by the equivalent stress with higher center frequency 6.0 MHz. Therefore, the laser-generated Rayleigh waves in the Ep/Al system with smaller coating thickness can be excited by the higher center frequency of the equivalent stress.

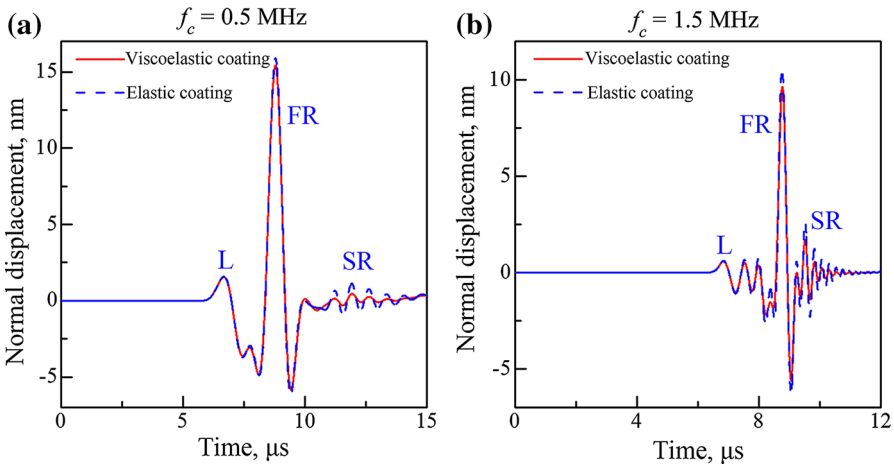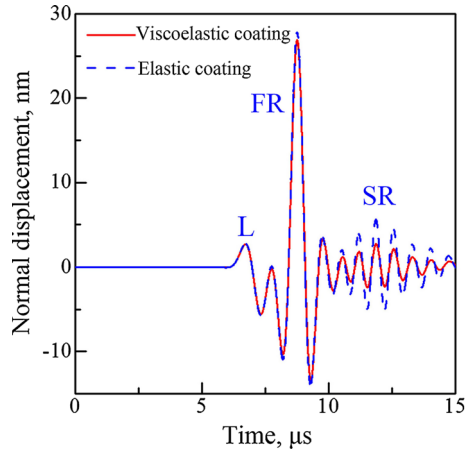**Fig. 7** Normal surface displacements with opaque Ep coating

Fig. 8 Normal surface displacements with different coating materials (a) perspex and (b) glass epoxy

We now discuss the transparency of the Ep coating. Figure 7 shows the normal surface displacements with an opaque Ep coating, and the other parameters are the same as those in Fig. 2b. Compared with the results with the transparent Ep coating (Fig. 2b), the attenuation and dispersive characteristics of the Rayleigh waves are similar, but the amplitudes of the Rayleigh waves are larger with opaque Ep coating in Fig. 7. This is because the exciting source is located on the surface of the Ep coating with the opaque property, and the energy of the Rayleigh waves is larger.

4.3 Influences of Different Coating Materials on Characteristics of Rayleigh Waves

We have also investigated the characteristics of the Rayleigh waves with different coating materials, such as perspex and glass epoxy, which are shown in Fig. 8a and

b, respectively. The material parameters were as follows $\rho = 1450 \, \text{kg} \cdot \text{m}^{-3}$, $C_{11}^* = 8.0 + \text{i}^*0.40$ GPa, $C_{22}^* = 8.0 + \text{i}^*0.40$ GPa, $C_{12}^* = 5.0 + \text{i}^*0.25$ GPa, and $C_{66}^* = 1.5 + \text{i}^*0.075$ GPa for perspex [22]; and $\rho = 1900 \, \text{kg} \cdot \text{m}^{-3}$, $C_{11}^* = 20.0 + \text{i}^*0.70$ GPa, $C_{22}^* = 50.0 + \text{i}^*2.5$ GPa, $C_{12}^* = 9.0 + \text{i}^*0.4$ GPa, and $C_{66}^* = 6.0 + \text{i}^*0.2$ GPa for glass epoxy [12]. The other structural parameters were the same as those in Fig. 2b, and the center frequency of the equivalent stress was 0.5 MHz for perspex and 1.5 MHz for glass epoxy. Figure 8a, b shows that the attenuation and dispersive characteristics of the Rayleigh waves are almost the same as those for the Ep coating (Fig. 2b), which indicates that the studies can be applied in evaluating mechanical properties of different types of coating/substrate systems.

5 Conclusion

In this work, we have established an FE model for the laser-generated Rayleigh waves and studied the propagation characteristics of the Rayleigh waves in an Ep/Al system, in which the viscoelasticity and transparency of the Ep are varied. The waveforms of the Rayleigh waves in the Ep/Al system consist of two parts, which is denoted as the FR and SR, respectively. The propagation characteristics of the SR are closely related to mechanical properties of the Ep coating. The attenuation of the SR becomes stronger with increasing viscoelastic moduli. With increasing elastic moduli, the velocity of the SR increases, but the dispersion characteristic of the SR becomes weaker and the attenuation of the SR decreases, this is because the center frequency of the SR increases. With increasing coating thickness, the dispersive characteristics of the SR become more apparent, while the attenuation of the SR decreases, this can be explained that the center frequency of the SR reduces. For a smaller coating thickness, the SR can be excited by the higher center frequency of the equivalent stress. Also, the transparency of the Ep coating affects the wave amplitudes. The study opens a prospect for using FE for extracting mechanical parameters and evaluating the adhesive quality of viscoelastic adhesive coating/substrate structures.

References

1. A. Cheng, T.W. Murry, J.D. Achenbach, J. Acoust. Soc. Am. **110**, 848 (2001)
2. Y.H. Liu, T.T. Wu, C.K. Lee, J. Acoust. Soc. Am. **111**, 2638 (2002)
3. H. Al-Qahtani, S.K. Datta, J. Appl. Phys. **96**, 3645 (2004)
4. X. Jian, Y. Fan, R.S. Edwards, S. Dixon, J. Appl. Phys. **100**, 064907 (2006)
5. X.D. Xu, J. Goossens, G. Shkerdin, C. Glorieux, IEEE Trans. Ultrason. Ferroelectr. Freq. Control **55**, 675 (2008)
6. P. Hess, A.M. Lomonosov, A.P. Mayer, Ultrasonics **54**, 39 (2014)

7. C. Grunsteidl, I.A. Veres, J. Roither, P. Burgholzer, T.W. Murray, T. Berer, Appl. Phys. Lett. **102**, 011103 (2013)
8. C. Ni, N. Chigarev, V. Tournat, N. Delorme, N. Chigarev, Z. Shen, V.E. Gusev, J. Appl. Phys. **113**, 014906 (2013)
9. J. Jia, Z.H. Shen, K.H. Sun, Appl. Opt. **54**, 7406 (2015)
10. S.I. Rokhlin, Y.J. Wang, J. Acoust. Soc. Am. **89**, 503 (1991)
11. K. Heller, L.J. Jacobs, J. Qu, NDT&E Int. **33**, 555 (2000)
12. M. Castaings, C. Bacon, B. Hosten, J. Acoust. Soc. Am. **115**, 1125 (2004)
13. H.X. Sun, B.Q. Xu, R.Z. Qian, J. Appl. Phys. **106**, 073108 (2009)
14. H.X. Sun, S.Y. Zhang, J. Appl. Phys. **108**, 123101 (2010)
15. H.X. Sun, S.Y. Zhang, Int. J. Thermophys. **34**, 1769 (2013)
16. H.X. Sun, S.Y. Zhang, J. Appl. Phys. **109**, 073107 (2011)
17. H.X. Sun, S.Y. Zhang, J.P. Xia, Int. J. Thermophys. **36**, 1156 (2015)
18. H.X. Sun, B.Q. Xu, H. Zhang, Q. Gao, S.Y. Zhang, Chin. Phys. B **20**, 14302 (2011)
19. H.X. Sun, S.Y. Zhang, S.Q. Yuan, Y.J. Guan, Y. Ge, Int. J. Thermophys. **37**, 68 (2016)
20. COMSOL Multiphysics User's Guide, Version 5.2. http://www.comsol.com/
21. O.M. Mukdadi, S.K. Datta, Rev. Prog. Quant. Nondestr. Eval. **23**, 238 (2004)
22. M. Castaings, M. Lowe, J. Acoust. Soc. Am. **123**, 696 (2008)